Double ferromagnetic resonance and configuration-dependent dipolar coupling in unsaturated arrays of bistable magnetic nanowires

J. De La Torre Medina* and L. Piraux
Institute of Condensed Matter and Nanosciences (ICMN), Université Catholique de Louvain, Place Croix du Sud 1, B-1348 Louvain-la-Neuve, Belgium

J. M. Olais Govea and A. Encinas†
Instituto de Física, Universidad Autónoma de San Luis Potosí, Av. Manuel Nava 6, Zona Universitaria, 78290 San Luis Potosí, SLP, Mexico

(Received 22 September 2009; revised manuscript received 17 March 2010; published 9 April 2010)

The ferromagnetic resonance properties in arrays of low diameter bistable nanowires have been studied. Measurements performed in the frequency swept mode show that in nonsaturated states, wires magnetized in the positive and negative direction absorb at different frequencies giving place to spectra with two absorption peaks. Moreover, the positive and negative wires obey different dispersion relations, which allow interpreting their different frequency-field dependence in terms of the uniform precession mode. Measurements along sets of first-order reversal curves allow to determine the dipolar interaction field as a function of the magnetic state. The configuration dependence of the interaction field is found to be proportional to the value of the dipolar interaction field of the saturated state. An analytical mean-field expression, which explicitly incorporates the dependence of the interaction field with the magnetic configuration, is proposed and used to obtain a general expression for both the effective field and the dispersion relation, which describes with remarkable agreement the ferromagnetic resonance measurements in saturated and nonsaturated states.

DOI: 10.1103/PhysRevB.81.144411 PACS number(s): 75.30.−m, 75.75.−c, 76.50.+g, 84.40.Az

I. INTRODUCTION

Since the discovery of the giant magnetoresistance effect 20 years ago,[1] nanomagnetism has been at the center of a great research interest and a considerable effort has been done in order to develop fundamental research and move new materials and effects toward applications. Two-dimensional (2D) arrays or assemblies of bistable magnetic particles are a class of systems which have received considerable attention due to the wide range of phenomena, properties, and potential use for novel concepts and applications.[2] For example, this type of materials have been proposed as storage media for perpendicular magnetic recording,[2–5] as the basis for magnetic quantum cellular automata,[6,7] and more complex electronic magnetic field coupled circuits.[8] A central problem related to any assembly of magnetic particles is the configuration-dependent dipolar interaction.[9–17] This is, in an array of particles, each one experiences the external applied field and the field created by neighboring particles and the value of this field depends explicitly on the exact configuration of all the particles in the array.

Experimentally, interparticle interactions of any particulate magnetic medium are not observable in magnetization cycles such as the major hysteresis loop but they may be evident in more complex magnetization processes.[18] Among which, those based on the Wohlfarth's remanence relation including Henkel, delta-M plots.[18] More recently, first-order reversal curves (FORCs) diagrams,[19] the $\Delta H(M,\Delta M)$ method,[20] and magnetic force microscopy[3,21,22] have also been proposed and used as methods to obtain more detailed information of the interparticle interaction. However, these methods only provide a qualitative picture of the configuration-dependent interaction field and more detailed information usually requires either complementary computer simulations or initial assumptions on the specific initial approximation.

Arrays of bistable magnetic nanowires (NWs) are a model system for studying magnetic interactions and switching behavior and have been proposed as candidates for ultrahigh storage densities.[4,5,23–35] These properties depend crucially on geometrical factors of the NW arrays, such as wire diameter, aspect ratio, and spacing between NWs.[36] Electrodeposition into nanoporous templates makes it possible to prepare a variety of NW arrays, and both their length and density can be controlled over a wide range. Furthermore, these NWs are parallel and their distribution can be random or quasiperiodic depending on the specific template used to grow them.[37] High aspect ratio particles combined with low-density arrays provide an easy way to obtain arrays of semi-isolated bistable magnetic NWs. In such arrays, each NW has only two stable states magnetized perpendicularly to the membrane, identical in magnitude but opposite in direction. In contrast, in high-density arrays of magnetic NWs, magnetostatic interaction becomes important and may even destroy the perpendicularly magnetized state.[38]

The present study reports the results of ferromagnetic resonance (FMR) measurements performed on arrays of bistable magnetic NWs. Among the most outstanding properties measured is the fact that in nonsaturated states, NWs magnetized in both the positive and negative directions have different resonance frequencies, hence, the FMR spectra are characterized by double absorption peaks. The field dependence properties of the resonance frequencies and the line shape are shown to depend on the specific magnetic state. Ferromagnetic resonance measurements along sets of first-order reversal curves in arrays of uniaxial bistable magnetic NWs lead to the first direct measurement of the configuration-dependent dipolar interaction. These results

 ©2010 The American Physical Society

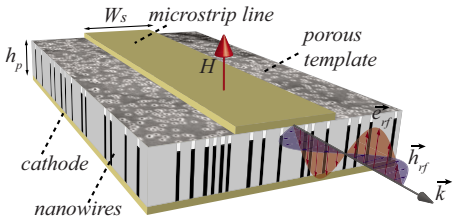

FIG. 1. (Color online) Schematics of the microstrip transmission line used in this study, in which the cathode, or ground plane, is separated from the 150-μm-wide microstrip line by a dielectric which corresponds to the 22-μm-thick polycarbonate membrane containing the nanowires.

permit to obtain an analytical mean-field expression for the configuration-dependent dipolar field which has been validated by predicting consistently the FMR measurements and by comparison with models reported in the literature.

II. EXPERIMENTAL DETAILS

Arrays of $Co_{55}Fe_{45}$ of 30 nm diameter and $Ni_{83}Fe_{17}$ of 40 nm diameter NWs with average length of $\approx 15-18$ μm and porosities of 5% and 3.4%, respectively;[39] have been grown by electrodeposition into the pores of 21-μm-thick lab-made track-etched polycarbonate (PC) membranes, in which the pores are parallel to each other but randomly distributed. These membranes have improved pore orientation, shape, size distribution, and surface roughness.[40] Full details of the preparation method can be found elsewhere.[37]

A Cr/Au layer is evaporated on one side of the membrane to serve as a cathode for electrodeposition and as the ground plane for the stripline. Electrodeposition is done at a constant potential of −0.9 V and −1.1 V vs a Ag/AgCl reference electrode from 40 g/l $FeSO_4$+80 g/l $CoSO_4$ +30 g/l H_3BO_3 and 5.56 g/l $FeSO_4$+131.42 g/l $NiSO_4$ +30 g/l H_3BO_3 electrolytes, respectively. The composition of the wires was checked by energy-dispersive x-ray analysis. Frequency swept FMR measurements were done using a 150-μm-wide stripline which was evaporated on the free surface of the membrane following electrodeposition, as depicted in Fig. 1.

In this configuration the microwave signal propagating along the microstip transmission line produces a microwave pumping field (h_{rf}, Fig. 1) which is perpendicular to the nanowires and induces a precession of the magnetization around the static equilibrium position. The transmission coefficient between 0 and 50 GHz is recorded by a Vector Network Analyzer while a constant magnetic field (H) is applied parallel to the NWs.[38] These measurements are then repeated at different H values between ± 10 kOe in order to obtain the frequency-field relation dispersion from the minimum of the absorption spectra. Magnetometry measurements were performed using an Alternating Gradient Magnetometer. All measurements in the present study have been done at room temperature.

III. SYSTEM CONSIDERATIONS

Low diameter, high aspect ratio NWs present a behavior close to that of an ideal infinite cylinder that has a square

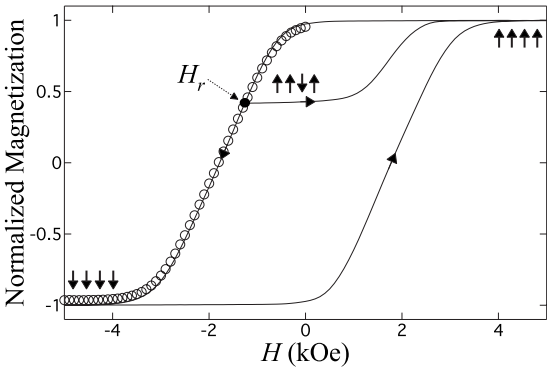

FIG. 2. Hysteresis loop (continuous line) and the corresponding dc demagnetizing remanence curve (open symbols) of the CoFe NW array measured with the field applied parallel to the NWs, and an intermediate nonsaturated state characterized by a minor loop generated with a negative H_r value.

hysteresis loop, the magnetization is bistable along the wire axis and has two equilibrium configurations, named here after positive m_+ and negative m_- with respect to the wire (easy) axis.[41,42] Nevertheless, the assembly of NWs obeys a coercive field distribution, which arises from inhomogeneities in features such as wire length, interwire distance, misalignment of the NWs, diameter dispersion, and specific microstructure of each wire.[22,36] During a cycle with H applied along the wire axis, the magnetization will reverse from the positive to negative saturation during the descending part, and from negative to positive saturation on the ascending part of the cycle. The reversal of the magnetization of the entire array from the saturated state to the other corresponds to the successive reversal of individual NWs.[19,22,43,44] Figure 2 shows the $m(H)$ loop for the CoFe NW array with H applied parallel to the NWs, where any magnetic state called hereafter m, can be written in terms of the fraction of m_+ and m_- wires, with $0 \leq m_\pm \leq 1$. The number of $m_\pm$ wires depends on the value of the applied field value H used to reach the magnetic state m so $m=m_+-m_-$. Moreover, since the number of NWs is constant, $m_++m_-=1$, $m_\pm$ can be obtained from the value of m as,

$$m_\pm = \frac{1 \pm m}{2}. \tag{1}$$

The extent to which the system behaves as an ideal bistable assembly can be evaluated by comparing the dc demagnetizing (dcD) remanence curve and the major hysteresis loop. This is shown in Fig. 2, were it can be observed that the dcD curve (symbols) overlaps with the corresponding part of the major hysteresis loop (continuous line), which supports the fact that the magnetization reversal of the entire array is done by the irreversible switching of individual wires.

In an array of *fully saturated* cylindrical NWs with saturation magnetization M_s, porosity P and no magnetocrystalline or magnetoelastic contributions, the effective field (H_{eff}) that includes the shape anisotropy ($2\pi M_s$) and the mean-field dipolar interaction, H_{D_0}, can be expressed as[38]

$$H_{eff} = 2\pi M_s - H_{D_0}, \tag{2}$$

where the dipolar interaction field in the saturated state is given by,[38,45]

$$H_{D_0} = 6\pi M_s P. \tag{3}$$

The effective field, Eq. (2), can eventually be extended to include magnetocrystalline or magnetoelastic effects. Each of these would be included as additive terms along with the magnetostatic field. Notice however, that neither of these effects have any influence on the dipolar interaction between wires, so for simplicity, CoFe and NiFe have been used in order to avoid such effects and simplify the analysis. In this case, the general form of the resonance condition for an array of NWs with the field applied parallel to the wire axis, provided that the system is saturated either positively or negatively, is given by the following linear-dispersion relation,[38]

$$f_{m_\pm} = \gamma(\pm H + H_{eff}), \tag{4}$$

where $f_{m_\pm}$ is the resonance frequency for positive (m_+) and negative (m_-) saturated NWs, γ the gyromagnetic ratio, and H the applied field parallel to the wires. The only difference in Eq. (4) for each population of wires is the change in sign in the slope, otherwise for a given applied field amplitude the same resonance frequency value is expected. Combining Eqs. (2) and (3) to rewrite Eq. (4) the explicit form of the dispersion relation for positive (m_+) and negative (m_-) saturated array of NWs with H applied parallel to the wires are given by

$$f_{m_+} = \gamma[H + 2\pi M_s(1 - 3P)], \tag{5}$$

$$f_{m_-} = \gamma[-H + 2\pi M_s(1 - 3P)]. \tag{6}$$

Both conditions are equivalent, however the magnetization will precess in opposite sense when subject to the same rf field, h_{rf}, perpendicular to the NWs, as illustrated schematically in Fig. 3. In the descending part of the cycle, Eq. (5) will be satisfied, while on the ascending part of the cycle, the FMR condition will be given by Eq. (6). The effective field in the saturated state [Eq. (2)] is obtained by fitting Eqs. (5) and (6) with data measured at saturation, moreover, since P is known, the value of M_s can be determined. Furthermore, if the system remains saturated when taken to the remanent state, the zero-field resonance frequency is $f_{H=0}=\gamma 2\pi M_s(1-3P)$. Besides, for positively and negatively magnetized isolated NWs the FMR f-H dependences are the same as Eqs. (5) and (6) with $P=0$, that is,

$$f_{m_+} = \gamma(H + 2\pi M_s), \tag{7}$$

$$f_{m_-} = \gamma(-H + 2\pi M_s). \tag{8}$$

Figure 3 shows the FMR response for the simple case of a system consisting of two noninteracting bistable NWs, namely, wire 1 and wire 2. The switching fields for wire 1 and wire 2 are, respectively, H_{sw_1} and H_{sw_2} and are such that $0<H_{sw_1}<H_{sw_2}$. Since the wires have different switching fields, the FMR properties of the ensemble are expected to depend on its magnetic configuration as the magnetic field is swept from one saturated state to the other. As the field is decreased from negative saturation to zero field and then increased to positive field values such that $H<H_{sw_1}$ [see Fig. 3(a)], the magnetization $\vec{M}$ and field $\vec{H}$ for both wires are parallel to each other. For this state, both wires are magnetized negatively and the precession of $\vec{M}$ around $\vec{H}$ is given in the same sense for both wires, so their resonance conditions correspond to Eq. (7). Particularly for the field values $-H_1$ and $-H_0$, the associated frequencies are, respectively, f_1 and f_0 and are such that $H_1>H_{sw_2}$ and $H_{sw_1}<H_0<H_{sw_2}$, as shown in Fig. 3(a). Increasing H up to H_0, the magnetization of wire 1 is reversed from the m_- state to the m_+ state. However, wire 2 remains magnetized negatively and its corresponding f-H dependence in the interval $H_{sw_1}<H<H_{sw_2}$ is still given by Eq. (5), with $f=f_0'$ for $H=H_0$.

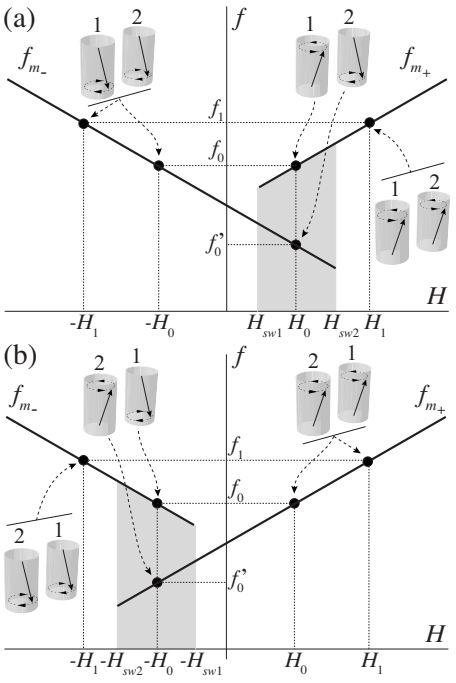

FIG. 3. Schematics of the linear-dispersion relation expected for NWs saturated in the positive and negative direction along the wires axis, where the external field is swept (a) from negative to positive saturation and (b) from positive to negative saturation.

Conversely, wire 1 is magnetized positively and $\vec{M}$ and $\vec{H}$ are parallel to each other. In this state the magnetization dynamics of wire 1 is equivalent to the one at $H=-H_0$ when it was magnetized negatively and $\vec{M}$ and $\vec{H}$ were also parallel to each other. Then, the associated resonance frequency is f_0, which corresponds to the frequency value at $H=|H_0|$ when both $\vec{M}$ and $\vec{H}$ are parallel to each other for wire 1, as shown in Fig. 3(a). This implies that in the field interval $H_{sw_1}<H<H_{sw_2}$, the f-H dependence of wire 1 is given by Eq. (8). In this field interval the wires have different resonance frequencies for the same applied field value and both resonance conditions of Eqs. (7) and (8) are satisfied. This means that one may expect to observe a double absorption in the FMR response for the whole NW array. As H is further increased to H_1, the magnetization of wire 2 is reversed from the negative to the positive state and its magnetization is now parallel to $\vec{H}$, which means that the corresponding f value is now f_1 for both wires and their f-H dependence is now given by Eq. (8).

Furthermore, if now the field is reversed from positive to negative saturation, the situation is inverted and wire 1 and

wire 2 will reverse their magnetizations at the fields $-H_{sw_1}$ and $-H_{sw_2}$, respectively. Therefore the double absorption is expected to be observed in the field interval from $-H_{sw_1}$ to $-H_{sw_2}$ as shown in Fig. 3(b). Extending this idea to an array of interacting bistable NWs, double resonance effects are to be expected when wires magnetized in both, positive and negative directions coexist. Moreover, from the schema in Figs. 3(a) and 3(b), it is clear that in order to measure the FMR properties of nonsaturated magnetic states, the swept frequency FMR is perfectly suited since the transmission coefficient is recorded as a function of the frequency while the system is subject to a homogeneous and constant magnetic field that assures the stability of the measured magnetic configuration. In the present study, frequency swept FMR measurements have been done over saturated as well as nonsaturated magnetic states in bistable NW arrays, which present non-negligible dipolar interactions between wires. In the following section, the main results are presented.

IV. EXPERIMENTAL RESULTS

The FMR study has considered measurements along the major hysteresis loop and first-order reversal curves varying the magnetic configuration. In the following, the reverse field H_r corresponds to the field at which the system is taken on the major loop in order to begin all FORC and remanence measurements.

A. Major loop measurements

Recording the FMR signal at different points over the major $m(H)$ loop, the absorption spectra as a function of the specific magnetic configurations can be observed. This is shown in Fig. 4 for the FMR signal for the CoFe NW array recorded at different values during the (a) descending and (b) ascending part of the cycle. As seen in Fig. 4, in nonsaturated states the FMR spectra shows two absorption peaks. Since the saturated state shows a single resonance peak, the presence of two absorptions in nonsaturated states are attributed to the FMR of NWs polarized in each of the two possible directions, that is, $m_{\pm}$, as discussed in detail below. Moreover, based on the $m(H)$ loop, it is possible to identify the correspondence of each peak to each polarization direction. In the descending part of the cycle, the initial saturated state is positive and reversal takes place for negative H_r values. Since at the beginning of reversal, the wires are mostly polarized in the positive direction, the highest intensity peak, which as seen in Fig. 4(a) in this case is the low-frequency peak, corresponds to the m_+ NWs, while the m_- NWs absorb at higher frequencies. Inversely, in the ascending part of the cycle, Fig. 4(b), the system is originally saturated in the negative direction and the nonsaturated region is reached with positive H_r values and the FMR peaks of each magnetization direction are now reversed. Moreover, as seen in Fig. 4, the relative intensity of the peaks change as a function of H_r. In particular, since the absorption or imaginary part of the susceptibility (χ'') is proportional to the net magnetization, the intensity of each peak is proportional to the corresponding number of m_+ and m_- NWs.[46] In the descending

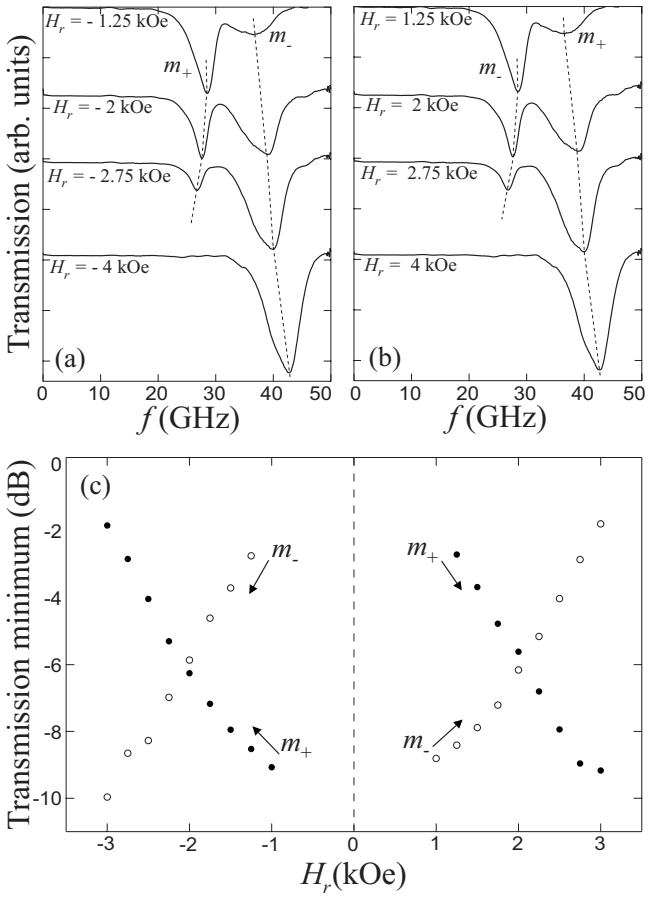

FIG. 4. FMR signal recorded at different H_r values during the (a) descending and (b) ascending parts of the cycle. (c) Transmission minimum of both the m_+ (filled symbols) and the m_- (empty symbols) NWs as a function of H_r for the ascending and descending parts of the cycle.

part of the cycle, Fig. 4(a), the intensity of the m_+ peak decreases while that of the m_- increases and the H dependence of each peak are opposite. Indeed, as the negative field increases, the resonance frequency of the m_- peak increases, while for the m_+ peak decreases, as shown by the dotted lines. By symmetry, measurements done with an opposite reverse field H_r of the same intensity, lead to identical spectra in which the higher- and lower-frequency peaks correspond now to the m_+ and m_- wires, respectively [Fig. 4(b)].

Figure 4(c) shows the maximum amplitude of the transmission coefficient plotted as a function of H_r for each resonance peak, measured during the ascending and descending part of the cycle. As seen in the figure, there is a clear correlation between the peak amplitude and the fraction of NWs magnetized in each the positive and negative direction. In the descending part of the cycle, reversal begins with negative H_r values with all the NWs magnetized in the positive direction and as H_r increases the number of m_+ NWs decreases while that of the m_- increases. During the ascending part of the cycle, reversal takes place with positive reverse fields, the behavior of the amplitude is the same, but the situation for the $m_{\pm}$ NWs is inverted. Since the number of NWs is constant, one peak will increase its amplitude while the other decreases until it vanishes once reversal concludes. The H

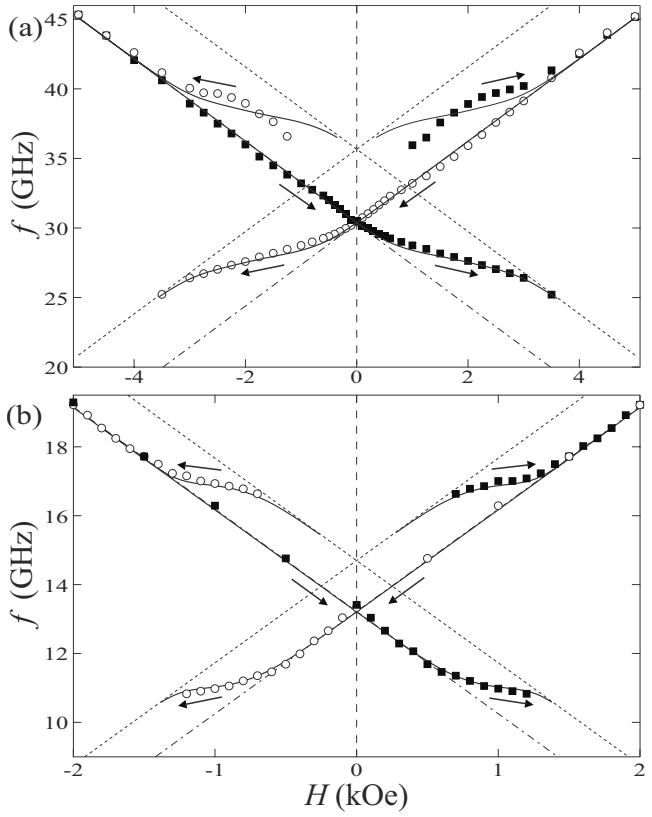

FIG. 5. Dispersion relations measured over the full hysteresis cycle in (a) CoFe and (b) NiFe NWs. Empty (filled) symbols correspond to the descending (ascending) part of the cycle. Included also the dispersion relations of the saturated array of interacting NWs (dash-dotted line), the noninteracting single NW (dotted line) and the calculated resonance frequencies based on Eqs. (14) and (15) (continuous line).

dependence of the peak amplitude is given by the variation in the magnetization with H, that is, by the $m(H)$ loop. This is further supported by the fact that both peaks have the same amplitude at a H value that corresponds to the coercive field ($H_c = \pm 2$ kOe) where $m_{\pm} = 0.5$.

B. Full dispersion relation

From the collection of all resonance frequencies at given applied field values, the dispersion relation for the entire major loop can be obtained, as shown in Figs. 5(a) and 5(b) for the CoFe and the NiFe samples, respectively. Clearly, the dispersion relation is linear as long as the system is saturated. Once reversal begins the field region where the double resonance occurs is also evidenced by the loss of linearity and the appearance of two different resonance frequencies for a single applied field value. In the field region where reversal takes place, a significant difference is evident between the experimental behavior shown in Fig. 5 and the simple schematic picture given in Fig. 3.

The resonance frequencies measured between saturation and zero field for both, positive and negative magnetization, have been fitted to Eqs. (5) and (6), respectively (dash-dotted lines), in order to obtain the value of the effective field. For the $Co_{55}Fe_{45}$ sample, $\gamma = 2.96$ GHz/kOe (Ref. 47) and $H_{eff} = 10.24$ kOe so for $P = 5\%$ one obtains the M_s value of 1917 emu cm^{-3}, which agrees well to the M_s value of 1881 emu cm^{-3} of the same alloy composition obtained from the Slater-Pauling curve for CoFe alloys.[48] For the $Ni_{83}Fe_{17}$ NWs, $\gamma = 2.97$ GHz/kOe, and $H_{eff} = 4.44$ kOe which yields a value of $M_s = 788$ emu/cm^3 for $P = 3.4\%$.

The departure of the resonance frequencies from the dispersion relation for the saturated state [dash-dotted lines in Figs. 5(a) and 5(b)] in the field interval where reversal takes place, are attributed to the changes in the effective field due to the configuration-dependent dipolar interaction field.[19,43] As seen in Figs. 5(a) and 5(b), in the field interval where both $m_{\pm}$ are present, the resonance frequencies are higher than the values expected for the saturated state, and are limited to the region comprised between the dispersion relation of Eqs. (5) and (6) (dash-dotted lines) and those of the single-isolated NW, Eqs. (7) and (8), (dotted lines).

From the dispersion relation and the expression for the effective field $[2\pi M_s - 6\pi M_s P]$ for the saturated state, it can be seen that an increase in the resonance frequency at a fixed H value with respect to the values corresponding to the saturated state [dash-dotted lines in Figs. 5(a) and 5(b)] can only be due to a lower value of the dipolar field ($H_D < 6\pi M_s P$). Indeed, as the dipolar field varies approaching the limit of the noninteracting isolated NW, the dispersion relation will shift upwards until it reaches the upper limit of the isolated wire (dotted lines). Observing the behavior of the resonance frequencies in the regions where reversal takes place in both parts of the cycle, one can notice that the resonance frequencies vary in opposite sense and follow the same behavior as $m_{\pm}$. For instance, in the descending part of the cycle, once reversal begins, the number of m_+ NWs decreases while those magnetized in the negative direction, m_- increases. As seen in Figs. 5(a) and 5(b), as the number of m_+ decreases, the corresponding resonance frequencies shift progressively from the dispersion relation of the positive fully saturated NW array (dash-dotted line with positive slope) toward the dispersion relation for the isolated NW magnetized in the positive direction (dotted line with positive slope), as a result of a decrease in the interaction field in positively magnetized NWs. On the other hand, as the number of m_- NWs increases, the resonance frequency shifts from the dispersion relation of the single NW magnetized in the negative direction (dotted line with negative slope) toward the dispersion relation of the negative fully saturated NW array (dash-dotted line with negative slope), consistent with an increase in the interaction field in negatively magnetized NWs.

As reversal is completed, the resonance frequency of the m_+ reaches the limit value of the isolated noninteracting NW, while for the m_-, it converges to the value corresponding to the saturated state. By symmetry, on the ascending part of the cycle, at positive H values, the same behavior is observed for an initial state saturated in the negative direction. The different frequency variation for the m_+ and m_- NWs suggest that the FMR is probing separately the interaction field experienced by each magnetization direction.

C. FMR first-order reversal curves

In order to determine magnetic parameters, specifically the effective field in nonsaturated states, measurement of the

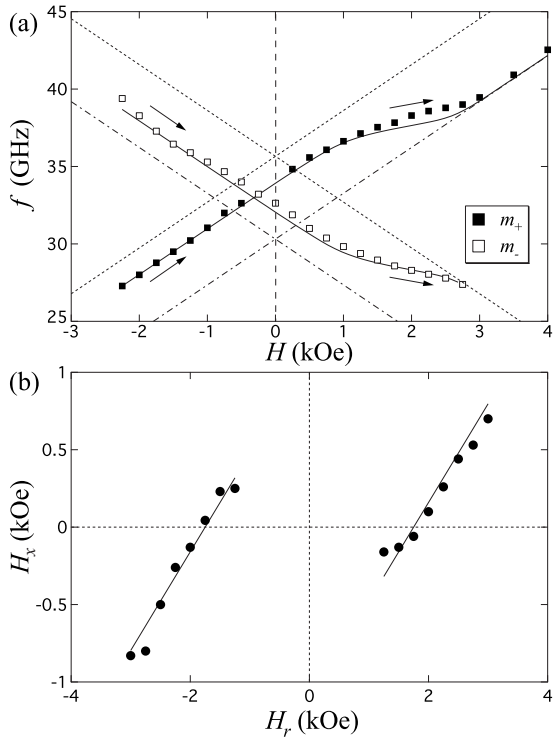

FIG. 6. (a) FMR-FORC measured on the CoFe sample with a reverse field of −2250 Oe, along with the theoretical dispersion relation of the saturated array of interacting NWs (dash-dotted line), the noninteracting single NW (dotted line) and the calculated resonance frequencies based on Eqs. (14) and (15) (continuous line). (b) Intersection field H_x as a function of the reverse field H_r. The calculated H_x field (continuous line) is obtained using Eq. (11) and the variation in m with H from the corresponding hysteresis loop.

FMR spectra along FORC have been done. The FMR-FORCs have been measured by applying first a large saturating magnetic field. Then the field is taken to a given reverse field H_r value in order to establish a nonsaturated configuration. Finally the system is subject to a field sequence back to the original saturated state while the FMR spectra are recorded at regular field increments. The following FORCs are measured similarly but with different reverse field values. The FMR-FORC dispersion relations are constructed from the collection of these spectra. Figure 6(a) shows a typical FMR-FORC dispersion relation for the CoFe NW array.

As seen in the figure, the FMR measurements provide the resonance frequency for both $m_\pm$ NWs so their field dependence can be followed separately. From these measurements it is observed that the initial state during the return to saturation is stable, as evidenced by the linear variation in the resonance frequency as a function of the applied field for both the $m_\pm$ NWs. This state persists up to a given positive field, then as the reversal toward the positive saturated state begins, a change in the slope is observed in both $f_{m_\pm}$ resonance frequencies. Finally, the saturated state is reached and a single resonance peak is observed which in this case corresponds to the NWs magnetized in the positive direction which follows the expected dispersion relation for the saturated state (dash-dotted line). On the other hand, as reversal is achieved, the number of negatively magnetized NWs tends to zero and their corresponding resonance frequency approaches that of the single isolated nanowire (dotted line).

Notice that as the field is increased from the reverse field H_r up to positive saturation, the field variation in the resonance frequency are opposite for each polarization direction. In this case, for the m_- NWs the frequency decreases as the field is increased, while for the m_+ NWs the resonance frequency increases with the field. An interesting property of these FMR-FORCs is that both dispersion relations intersect at a field value which depends on the magnetic configuration, as shown in Fig. 6(b), which shows the intersection field H_x measured from FMR-FORCs at different reverse field values. As seen in the figure, this intersection field takes both positive and negative values and is equal to zero when the reverse field is equal to the coercive field.

V. CONFIGURATION-DEPENDENT DIPOLAR INTERACTION

As suggested by the results shown in previous sections, the loss of linearity of the resonance frequencies in nonsaturated states is related to the configuration-dependent dipolar interaction field between the wires which changes at every field value, that is, the second term in Eq. (2) changes with the configuration. To quantify this configuration dependence, the measurement of frequency swept FMR-FORCs is very appealing since it allows to measure the spectra of a given magnetic state while subject to a constant applied magnetic field and from the corresponding resonance frequencies, the FMR-FORC dispersion relation for the $m_\pm$ NWs is obtained. In this sense, measurement of the FMR-FORCs allows to explore specific nonsaturated states based on sets of dispersion relations for each $m_\pm$ magnetization direction.

The interaction field experienced by each magnetization direction in a given nonsaturated configuration, $H_{D_\pm}$, can be determined by fitting the linear part of each $m_\pm$ FORC to an expression analogous to Eq. (4), but allowing the dipolar interaction term to vary, that is,

$$f_{m_\pm} = \gamma(\pm H + H_{eff_\pm}). \tag{9}$$

Each fit provides the effective field for the corresponding magnetic configuration for each magnetization direction, $H_{eff_\pm}$, and the dipolar interaction field is obtained by subtracting the shape anisotropy contribution, $H_{D_\pm} = 2\pi M_s - H_{eff_\pm}$. Figure 7 shows the dipolar interaction field for the CoFe sample in units of $(6\pi M_s P)$ as a function of the reverse field H_r compared to the fraction of $m_\pm$ wires and their field dependence as obtained from the normalized hysteresis loop. Clearly, the variation in the interaction field is proportional to the fraction of NWs and its value changes from a maximum of $H_{D_0} = 6\pi M_s P$ which corresponds to the case of the saturated state [Eq. (3)], and tends toward a minimum of zero as the fraction of $m_\pm$ NWs tends to zero, which corresponds to the limit of an isolated nanowire. From these results and Eqs. (1) and (3), the dipolar interaction field for an arbitrary nonsaturated state can be rewritten to take into account explicitly the dependence on the magnetic state, that is,

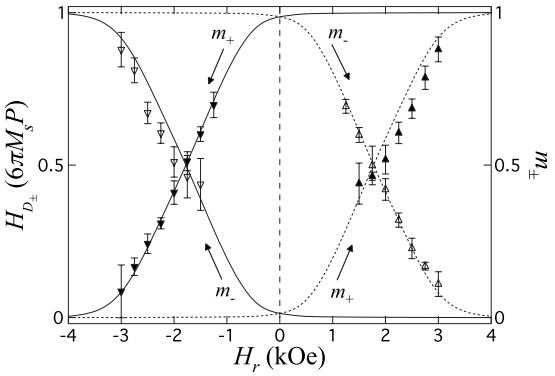

FIG. 7. Dipolar interaction field in units of $6\pi M_s P$ as a function of the reverse field compared to the fraction of $m_\pm$ NWs obtained from the $m(H)$ loop and shown in dotted lines for the CoFe sample.

$$H_{D_\pm} = H_{D_0} m_\pm = \frac{1}{2} H_{D_0} \pm \frac{1}{2} H_{D_0} m. \tag{10}$$

The reliability of the parameters obtained from the FMR-FORCs depends on having a finite field interval where the magnetization remains stable when the field is swept from H_r toward the saturated state, so there is a finite region where the FMR-FORC is linear and Eq. (9) can be used. Equation (10) provides separately the values of the interaction field for each magnetization direction. Physically, these expressions provide the dipolar field experienced by a single wire polarized in a given direction (positive or negative) due only to the rest of the wires polarized in the same direction. This is concluded based on the results shown in previous sections which clearly indicate that in nonsaturated states each absorption peak are only related to those NWs in each magnetization direction. So the resonance frequencies are given only in terms of the corresponding effective fields, as stated in Eq. (9). Moreover, from Eq. (10) and the results shown in Fig. 7, this description leads to a situation in which there are two different values of the interaction field (H_{D+} and H_{D-}) for a given magnetic state. Although this is physically plausible, as mentioned above, one would expect that the more general case is such that for a given magnetic state corresponds a single value for the dipolar interaction.

In this sense, any arbitrary state is characterized by an effective interaction field which is defined as the sum of the stray field produced by the $m_\pm$ wires. At the coercive field $m=0$ and, by definition, the effective interaction field is also equal to zero. For any other state, there will be an imbalance between $m_\pm$, and the effective interaction will be different from zero. This imbalance is given by m and as seen in Eq. (10), the first term $(H_{D_0}/2)$ is constant and corresponds to the value at the coercive field for each population of wires, while the excess field is given by the second term. In other words, if the zero is taken at the coercive field the imbalance in field provided by the second term corresponds to the configuration-dependent dipolar interaction field, which reads

$$H_{int} = \frac{1}{2} H_{D_0} m. \tag{11}$$

Physically, this expression provides the value of the interaction field at a given magnetic state m which corresponds to the field experienced by a single wire due to the rest of the NWs in the array. As suggested by Eq. (10) the value of this interaction field is obtained from the results shown in Fig. 7 as $(H_{D_+} - H_{D_-})/2$ for each reverse field value. Moreover, from the hysteresis loop the correspondence between m and the reverse field is known, which allows to plot this field for any system, for which H_{D_0} is known, in a single straight line in units of $H_{D_0}/2$ plotted as a function of m, as shown in Fig. 8 for the CoFe and NiFe samples.

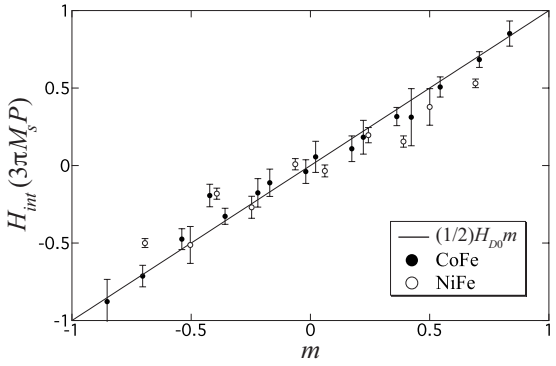

FIG. 8. Interaction field H_{int} in units of $H_{D_0}/2$ as a function of the magnetic state m. The continuous line corresponds to Eq. (11).

VI. DISCUSSION AND VALIDATION

In the previous section, an analytical expression has been obtained for the configuration-dependent dipolar interaction and two forms of expressing this interaction field have been presented, Eqs. (10) and (11). However, these expressions have different physical meaning, while Eq. (10) expressed in terms of $m_\pm$, provides the field experienced by a single wire due only to the rest of the wires magnetized in the same direction, Eq. (11) expressed as a function of m provides the field experienced by a single wire due to the rest of the wires in the array independently of their magnetization. So the general form of the interaction field corresponds to Eq. (11) from which Eq. (10) can be derived, and their usage depends on whether the system is analyzed in terms of $m_\pm$ or m. This subtlety is very important since both Eqs. (10) and (11) yield different values for the interaction field for any state and particularly in the saturated state. Indeed, at saturation Eq. (10) give H_{D_0} for one magnetization direction and zero for the other direction while Eq. (11) gives $1/2H_{D_0}$. However, this difference results from the variables used to express the interaction field. Indeed, while the fraction of wires are such that $0 \leq m_\pm \leq 1$, the normalized magnetization $m=m_+-m_-$ is such that $-1 \leq m \leq 1$. When the total magnetization goes from one saturated state to the other, $\Delta m_\pm = |1|$ and $\Delta m = |2|$. Moreover, measurements done on the saturated state by definition only probe the magnetic properties of a single magnetization direction, which is why the value measured in the saturated state for the dipolar interaction field is given by H_{D_0} consistent with Eq. (10) and in agreement with Ref. 38.

Considering the general form of the interaction field, Eq. (11), this expression can be related to the phenomenological

mean-field expression widely used for the configuration-dependent dipolar interaction[9,12,13,49,50]

$$H_{int} = \alpha m, \tag{12}$$

where α is a phenomenological parameter that needs to be determined. Furthermore, even after its value is determined, it provides no physical insight. However, comparing this expression with Eq. (11) the interaction parameter α can be identified as one half of the interaction field in the saturated state H_{D_0}.

In this sense, Eq. (11) is a very general result since this expression is valid for any array of identical bistable objects having a unique and common easy axis. Indeed, analytical mean-field expressions for H_{D_0}, the mean-field dipolar interaction in the saturated state, can be calculated for several common geometries.[51,52] Moreover, H_{D_0} can be obtained from the effective field of the system [Eq. (2)] which can be measured by numerous techniques since, in a purely magnetostatic system (no magnetoelastic or magnetocrystalline anisotropies), it corresponds to the effective magnetic anisotropy of the array.[38] Clearly the validity of Eq. (11) is limited to low and moderate densities where the mean-field approach is known to be valid and the interaction field in the saturated state is low enough to avoid collective or cooperative behavior.[38,53]

Based on these results, the effective field can be generalized for the case of a single wire that interacts with the rest of the NWs in the array, which includes the configuration-dependent interaction field. Using Eq. (3) and by substitution of the second term in Eq. (2) with Eq. (10), one obtains

$$H_{eff_{\pm}} = 2\pi M_s \left[1 - \frac{3}{2} P(1 \pm m) \right]. \tag{13}$$

Using this expression, the dispersion relation can be extended to incorporate explicitly the configuration-dependent interaction field. Rewriting Eqs. (5) and (6) yields,

$$f_{m_+} = \gamma H + 2\pi M_s \gamma \left[1 - \frac{3}{2} P(1 + m) \right], \tag{14}$$

$$f_{m_-} = -\gamma H + 2\pi M_s \gamma \left[1 - \frac{3}{2} P(1 - m) \right]. \tag{15}$$

These equations have been used to calculate the resonance frequencies for the full cycle dispersion relation and the FMR-FORCs. The calculations require the values of m at each field point which are obtained from the hysteresis loop as well as knowledge of P and M_s. The results are shown in Figs. 5(a), 5(b), 6(a), and 6(b) as continuous lines. In all cases, a remarkable agreement is found between the measured and calculated resonance frequencies. Notice that with the incorporation of the configuration dependence, the entire cycle as well as minor loops are obtained from a single expression, which provides evidence of the validity of Eq. (11). In this sense, Eqs. (14) and (15) correspond to the generalized dispersion relation which accounts for both saturated and nonsaturated states. In particular, these equations reduce to Eqs. (5) and (6) in the saturated states $m = \pm 1$ and to Eqs. (7) and (8) in the saturated states $m = \mp 1$, respectively. Moreover, Eq. (13) can be extended to allow for other contributions to the effective field such as magnetocrystalline or magnetoelastic effects. Indeed, other contributions to H_{eff} are additive to the magnetostatic terms. In this sense, extension of the effective field to include either magnetocrystalline or magnetoelastic effects have been done for arrays of nanowires in Refs. 54 and 55. However, since the present study is focused on the determination of the configuration-dependent dipolar interaction, magnetoelastic and magnetocrystalline anisotropy contributions have been intentionally avoided by selecting materials for which these contributions are negligible at room temperature.[55]

To further corroborate these expressions, it is straightforward to show that the intersection coordinates for the dispersion relations in a given FORC, obtained by solving Eqs. (14) and (15), are such that the intersection field H_x is given by Eq. (11) and the intersection frequency, f_x, is

$$f_x = \gamma \left(2\pi M_s - \frac{H_{D_0}}{2} \right). \tag{16}$$

First, the fact that H_x is given by Eq. (11) corroborates that the interaction field acts as a bias field superposed to the applied field. Indeed, this field corresponds to the shift along the field axis which is proportional to the difference between the number of wires magnetized in the positive and negative directions. In Fig. 6(b) the calculated intersection field, H_x, obtained using Eq. (11) and the $m(H)$ values measured from the normalized hysteresis loop, is compared against the measured one, and a very good agreement is found.

More surprising is the fact that the intersection frequency [Eq. (16)] is constant and does not depend on the magnetic configuration and it corresponds to the resonance frequency at the coercive field, $m=0$. Indeed, the first term in Eq. (16), $2\pi M_S \gamma$, corresponds to the resonance frequency of the isolated nanowire at remanence, while the second term, $(1/2)H_{D_0}\gamma$, can be identified from Eq. (10) and corresponds to a frequency shift produced by a field equal to one half of the interaction field measured at saturation ($m_{\pm}=1/2$ or $m=0$). In this sense, the constant intersection frequency given by Eq. (16) corresponds to a horizontal line that crosses the frequency axis at a value placed midway between the isolated nanowire and the fully saturated array of nanowires.

The validity of Eq. (11) has been further corroborated by comparison with recent results on the dipolar interactions in bistable Co NW arrays grown in ordered anodized alumina templates.[36] In this paper, the interaction field in the limit of the saturated state was found to be 1.5 kOe using in-field magnetic force microscopy for an array of Co NWs having a pitch length $a=100$ nm and wire diameter $d=30$ nm. This value is in fair agreement with the value of ≈ 1.1 kOe obtained using Eq. (11) and the relation $P=\pi(d/a)^2/(2\sqrt{3})$ for the porosity in hexagonally arranged array of NWs with the same values of a and d.

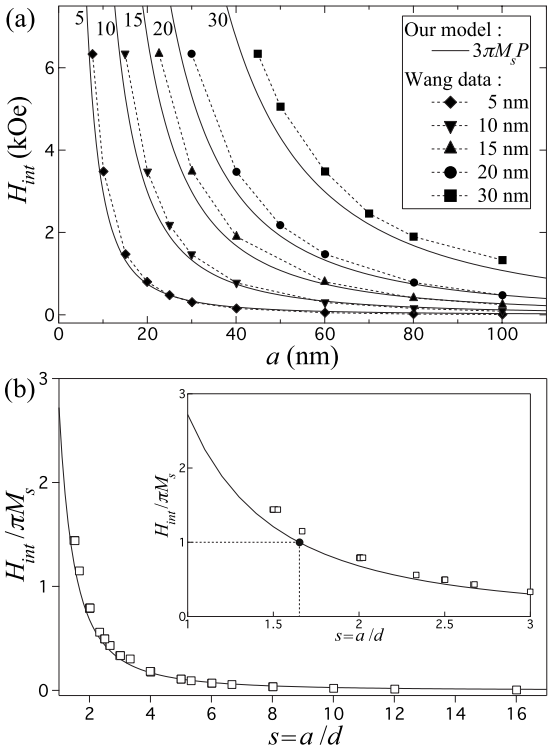

FIG. 9. (a) Calculated interaction field H_{int} at saturation from Eq. (17) as a function of the average pitch length a for wire diameters $d=5$, 10, 15, 20, and 30 nm (from left to right as continuous lines with numbers). For each wire diameter the model is compared with data from Wang, *et al.* (Ref. 36) (symbols). (b) Calculated dipolar field as a function of the ratio between the pitch length and wire diameter, $s=a/d$ expressed in units of πM_S, symbols correspond to values obtained from Ref. 36.

On the other hand, a simple computational model has also been reported by Wang, *et al.*[36] In this sense, an analytical expression for the configuration-dependent dipolar interaction field in the mean-field approach for an hexagonally ordered array of NWs can be obtained combining Eqs. (3) and (11) with the explicit form for P, that is,

$$H_{int} = \frac{\sqrt{3}}{2}\pi^2 M_s \left(\frac{d}{a}\right)^2 m. \tag{17}$$

This expression depends only on the magnetic material (M_s), wire diameter d, and average interwire distance or pitch length a. The variation in H_{int} in the limit of $m=1$ as a function of a is shown in Fig. 9(a) as continuous lines for wire diameters of $d=5$, 10, 15, 20, and 30 nm (indicated as numbers). As expected, for each diameter considered, the dipolar interaction field decreases asymptotically to zero as a increases. As seen from Fig. 9(a) the variation in H_{int} vs a for each wire diameter is in very good agreement with the results reported by Wang, *et al.*[36] for the dipolar field at saturation (symbols), which shows that Eqs. (11) and (17) are correct expressions for H_{int}.

The previous results can be extended to a more general case by using the ratio between the pitch length and wire diameter, $s=a/d$ and expressing the field in units of πM_s so it becomes material independent. Figure 9(b) shows this calculation using Eq. (17) for $m=1$ and compared with the data of Wang, *et al.*[36] (open symbols). Again, a very good agreement is found in the entire range of values considered for s, even at low values as shown in the inset. Similarly to the results shown in Fig. 9(a) for Co NWs, the interaction field falls off as $1/s^2$ as the interwire distance is increased from the limit of touching wires ($s=1$) to large interwire separation. Furthermore, it is well known that bringing the NWs closer leads to a rotation of the easy axis from parallel to perpendicular to the wire axis. In a previous report it has been shown using Eqs. (2) and (3) that the critical value at which the array becomes isotropic, $H_{eff}=0$ is $P=1/3$.[38] As mentioned before, this result is valid for a single population of wires in the saturated state, which follows directly from Eq. (13) when $m=1$. However, since the general expression for the interaction field, Eq. (11), is different; it is worth to establish its corresponding value for the critical porosity. By setting $P=1/3$ and $m=1$ in Eq. (13) and comparing with Eq. (11), the critical value of the interaction field is $H_{int}=\pi M_s$, which for the case considered in Fig. 9(b) is obtained, using Eq. (17), when $s^2=\pi\sqrt{3}/2 (s=1.65)$.

It is interesting to notice that despite the fact that Eq. (11) is a mean-field expression deduced from measurements done on an array of parallel NWs but randomly distributed, a very good agreement is found when compared to the case of an ordered array of NWs. This feature is attributed to the fact that for the densities considered the spatial mean-field average used implicitly in Eq. (11) will not be too different from the averaging done by the explicit summation of dipolar fields as done in Ref. 36. In the FMR experiment the absorption spectra represents a distribution of resonance frequencies, so a reduction in the dispersion of interwire distances and wire diameters is expected to lead a reduction in the dipolar field dispersion, which in turn leads to a reduction in the dispersion of resonance frequencies or a reduction in the linewidth of the absorption spectra. Then, the resonance frequency will remain unchanged because it represents an average, which further supports the fact that H_{int} can accurately be approximated in terms of the expression of P for and hexagonally arranged NW array as seen from Eq. (17). The agreement observed in Fig. 9 further supports the validity of Eq. (13) and, in particular, confirms the correctness of Eq. (3) for the dipolar interaction field at saturation for a single polarization direction, which has recently been reconsidered by several authors.[56–58]

VII. CONCLUSIONS

In conclusion, the FMR absorption properties of bistable magnetic NWs have been studied. The possibility to obtain magnetic states with NWs magnetized in both the positive and negative direction leads to double FMR absorption peaks. The H dependence of the resonance frequencies show that each magnetization direction follows different dispersion relations and their respective peak intensity is proportional to the fraction of NWs magnetized in each direction. The configuration-dependent dipolar interaction field in nonsat-

urated states has been measured using FMR-FORCs and an analytical mean-field expression, which explicitly incorporates the dependence of the interaction field with the magnetic configuration, has been proposed and validated. These results are of great relevance as they offer a simple model which is potentially suitable for a wide range of 2D-magnetic systems and specific applications, such as magnetic recording, determination of the intrinsic switching field distribution and magnetic quantum cellular automata.

ACKNOWLEDGMENTS

The authors thank R. Legras and E. Ferain for providing the PC membranes. This work was partly supported by the Interuniversity Attraction Poles Program (P6/42)–Belgian State–Belgian Science Policy. A.E. thanks CONACYT for financial support through Grants No. 50650 and No. 48436 as well as UCL. J.M.O.G. is grateful to COPOCYT and SIP-UASLP for financial support.

*Corresponding author; joaquin.delatorre@uclouvain.be
†Corresponding author; aencinas@ifisica.uaslp.mx

[1] M. N. Baibich, J. M. Broto, A. Fert, F. Nguyen Van Dau, F. Petroff, P. Etienne, G. Creuzet, A. Friederich, and J. Chazelas, Phys. Rev. Lett. **61**, 2472 (1988).
[2] C. A. Ross, Annu. Rev. Mater. Sci. **31**, 203 (2001).
[3] J. I. Martín, J. Nogués, K. Liu, J. L. Vicent, and I. K. Schuller, J. Magn. Magn. Mater. **256**, 449 (2003).
[4] B. Cui, W. Wu, L. Kong, X. Sun, and S. Y. Chou, J. Appl. Phys. **85**, 5534 (1999).
[5] T. Savas, M. Farhoud, M. Hwang, H. Smith, and C. A. Ross, J. Appl. Phys. **85**, 6160 (1999).
[6] R. P. Cowburn and M. E. Welland, Science **287**, 1466 (2000).
[7] A. J. Bennett and J. M. Xu, Appl. Phys. Lett. **82**, 3304 (2003).
[8] A. Imre, G. Csaba, L. Ji, A. Orlov, G. H. Bernstein, and W. Porod, Science **311**, 205 (2006).
[9] E. Kneller, J. Appl. Phys. **39**, 945 (1968).
[10] P. Smaller and J. S. Newman, IEEE Trans. Magn. **6**, 804 (1970).
[11] H. N. Bertram and A. K. Bhatia, IEEE Trans. Magn. **9**, 127 (1973).
[12] E. Della Torre, IEEE Trans. Audio Electroacoust. **14**, 86 (1966).
[13] G. Bertotti, *Hysteresis in Magnetism* (Academic Press, London, 1998).
[14] M. Fearon, R. W. Chantrell, and E. P. Wohlfarth, J. Magn. Magn. Mater. **86**, 197 (1990).
[15] E. P. Wohlfarth, J. Appl. Phys. **35**, 783 (1964).
[16] W. F. Brown, Jr., *Magnetostatic Principles in Ferromagnetism* (North-Holland, Amsterdam, 1962), pp. 112–118.
[17] M. Beleggia and M. De Graef, J. Magn. Magn. Mater. **285**, L1 (2005).
[18] A. Stancu, J. Optoelectron. Adv. Mater. **4**, 217 (2002).
[19] C. R. Pike, C. A. Ross, R. T. Scalettar, and G. Zimanyi, Phys. Rev. B **71**, 134407 (2005).
[20] A. Berger, B. Lengsfield, and Y. Ikeda, J. Appl. Phys. **99**, 08E705 (2006).
[21] J. Escrig, D. Altbir, M. Jaafar, D. Navas, A. Asenjo, and M. Vázquez, Phys. Rev. B **75**, 184429 (2007).
[22] C. A. Ross, M. Hwang, M. Shima, J. Y. Cheng, M. Farhoud, T. A. Savas, H. I. Smith, W. Schwarzacher, F. M. Ross, M. Redjdal, and F. B. Humphrey, Phys. Rev. B **65**, 144417 (2002).
[23] L. Spinu, A. Stancu, C. Radu, F. Li, and J. B. Wiley, IEEE Trans. Magn. **40**, 2116 (2004).
[24] T. G. Sorop, K. Nielsch, P. Goring, M. Kroll, W. Blau, R. B. Wehrspohn, U. Gosele, and L. J. de Jongh, J. Magn. Magn. Mater. **272-276**, 1656 (2004).
[25] M. Vazquez, K. Nielsch, P. Vargas, J. Velazquez, D. Navas, K. Pirota, M. Hernandez-Velez, E. Vogel, J. Cartes, R. B. Wehrspohn, and U. Gosele, Physica B **343**, 395 (2004).
[26] P. S. Fodor, G. M. Tsoi, and L. E. Wenger, J. Appl. Phys. **93**, 7438 (2003).
[27] M. Vazquez, K. Pirota, J. Torrejon, D. Navas, and M. Hernandez-Velez, J. Magn. Magn. Mater. **294**, 174 (2005).
[28] I. Dumitru, F. Li, J. B. Wiley, D. Cimpoesu, A. Stancu, and L. Spinu, IEEE Trans. Magn. **41**, 3361 (2005).
[29] P. Tomczak and A. R. Ferchmin, J. Magn. Magn. Mater. **306**, 228 (2006).
[30] M. Pardavi-Horvath, P. E. Si, M. Vazquez, W. O. Rosa, and G. Badini, J. Appl. Phys. **103**, 07D517 (2008).
[31] P. S. Fodor, G. M. Tsoi, and L. E. Wenger, J. Appl. Phys. **103**, 07B713 (2008).
[32] R. Lavin, J. C. Denardin, J. Escrig, D. Altbir, A. Cortes, and H. Gomez, IEEE Trans. Magn. **44**, 2808 (2008).
[33] O. C. Trusca, D. Cimpoesu, J. H. Lim, X. Zhang, J. B. Wiley, A. Diaconu, I. Dumitru, A. Stancu, and L. Spinu, IEEE Trans. Magn. **44**, 2730 (2008).
[34] B. Nam, B. Y. H. Choa, S. T. Oh, S. K. Lee, and K. H. Kim, IEEE Trans. Magn. **45**, 2777 (2009).
[35] L. Clime, P. Ciureanu, and A. Yelon, J. Magn. Magn. Mater. **297**, 60 (2006).
[36] T. Wang, Y. Wang, Y. Fu, T. Hasegawa, H. Oshima, K. Itoh, K. Nishio, H. Masuda, F. S. Li, H. Saito, and S. Ishio, Nanotechnology **19**, 455703 (2008).
[37] L. Piraux, A. Encinas, L. Vila, S. Mátéfi-Tempfli, M. Mátéfi-Tempfli, M. Darques, F. Elhoussine, and S. Michotte, J. Nanosci. Nanotechnol. **5**, 372 (2005).
[38] A. Encinas-Oropesa, M. Demand, L. Piraux, I. Huynen, and U. Ebels, Phys. Rev. B **63**, 104415 (2001).
[39] The porosity P is defined as the surface filling fraction and is obtained as the product of the density of pores and the pore diameter. The average interwire distance lies in the range 250–300 nm.
[40] E. Ferain and R. Legras, Nucl. Instrum. Methods Phys. Res. B **131**, 97 (1997).
[41] T. G. Sorop, C. Untiedt, F. Luis, M. Kroll, M. Rasa, and L. J. de Jongh, Phys. Rev. B **67**, 014402 (2003).
[42] R. Hertel, J. Appl. Phys. **90**, 5752 (2001).
[43] I. Dumitru, D. D. Sandu, and C. G. Verdes, Phys. Rev. B **66**, 104432 (2002).
[44] D. Grundler, G. Meier, K.-B. Broocks, Ch. Heyn, and D. Heitmann, J. Appl. Phys. **85**, 6175 (1999).
[45] L.-P. Carignan, C. Lacroix, A. Ouimet, M. Ciureanu, A. Yelon, and D. Menard, J. Appl. Phys. **102**, 023905 (2007).

[46] A. G. Gurevich and G. A. Melkov, *Magnetization Oscillations and Waves* (CRC, New York, 1996), pp. 10–29.
[47] F. Schreiber, J. Pflaum, Z. Frait, Th. Mühge, and J. Pelzl, Solid State Commun. **93**, 965 (1995).
[48] R. M. Bozorth, *Ferromagnetism* (D. Van Nostrand Company, Princeton, NJ, 1961), pp. 190–195.
[49] F. Liorzou, B. Phelps, and D. Atherton, IEEE Trans. Magn. **36**, 418 (2000).
[50] D. C. Jiles and D. L. Atherton, J. Magn. Magn. Mater. **61**, 48 (1986).
[51] U. Netzelmann, J. Appl. Phys. **68**, 1800 (1990).
[52] J. Dubowik, Phys. Rev. B **54**, 1088 (1996).
[53] A. H. Thomas, R. W. Chantrell, M. El-Hilo, P. W. Haycock, and K. O'Grady, J. Magn. Magn. Mater. **151**, 54 (1995).
[54] M. Darques, L. Piraux, A. Encinas, A. Popa, P. Bayle-Guillemaud, and U. Ebels, Appl. Phys. Lett. **86**, 072508 (2005).
[55] J. De La Torre Medina, M. Darques, and L. Piraux, J. Phys. D **41**, 032008 (2008).
[56] M. Vázquez, M. Hernández-Vélez, K. Pirota, A. Asenjo, D. Navas, J. Velásquez, P. Vargas, and C. Ramos, Eur. Phys. J. B **40**, 489 (2004).
[57] E. Padrón Hernández, S. M. Rezende, and A. Azevedo, J. Appl. Phys. **105**, 07B525 (2009).
[58] E. Padrón Hernández, A. Azevedo, and S. M. Rezende, J. Appl. Phys. **103**, 07D506 (2008).